

A Novel Numerical Algorithms Optimization Method with Machine Learning Frameworks: Application on Real-time Plasmas Equilibrium Reconstruction in EXL-50U Spherical Torus

G.H. Zheng^{1,4}, S.F. Liu^{1*,2}, X. Gu^{3†}, Y.P. Zhang³, J. Li³, Y. Liu³, X.C. Lun³, L. Xing³, J.G. Chen³, Z.Y. Chen³, Y. Yu³, D. Guo³, Z.Y. Yang⁴, H.S. Xie³, X.M. Song³, Y.J. Shi³ and EXL-50U Team

¹ School of Physics, Nankai University, Tianjin 300071, People's Republic of China

² Academy for Advanced Interdisciplinary Studies, Nankai University, Tianjin 300071, People's Republic of China

³ ENN Science and Technology Development Co., Ltd., Langfang 065001, People's Republic of China

⁴ Southwestern Institute of Physics, Chengdu 610041, People's Republic of China

*Email : lsfnk@nankai.edu.cn

†Email : guxiangc@enn.cn

This work proposes for the first time a novel optimization method for numerical algorithms, which takes advantages of machine learning frameworks PyTorch and TensorRT, leveraging their modularity, low development threshold, and automatic tuning characteristics to achieve a real-time plasmas reconstruction algorithm called PTEFIT as an application in tokamak-based controlled fusion that combines performance, flexibility, and usability. The algorithm has been deployed and routinely operated on the EXL-50U spherical tokamak, with an average inference time of only 0.268ms per time slice at 129×129 resolution, and has successfully driven feedback control of the maximum radial position of plasmas and iso-flux control. We believe that its design philosophy has sufficient potential to accelerate development and optimization in GPU parallel computing, and is expected to be extended to other numerical algorithms.

Keywords: Numerical optimization, Tokamak equilibrium, Real-time reconstruction, Feedback control

I. INTRODUCTION

Traditional numerical computation based on the first principle method always leads to unacceptable time complexity. Although with the rapid development of computation hardwares, it is a feasible way to accelerate relevant algorithms in parallel on GPUs, common researchers still struggle against the high threshold in complex optimization strategies on GPU programming.

In this case, machine learning is currently considered as the surrogates for high-fidelity, physical based algorithms. Trained machine learning models are almost entirely composed of matrix multiplication operations, whose computational speed can be significantly improved by parallel optimization. Furthermore, current machine learning frameworks have mature optimizations for various operators and easy to use, some of them even support automatic optimization of computational graphs and kernel functions to achieve maximum instruction throughput, cache hit rate, memory access efficiency, and thread utilization. However, although surrogate models often demonstrate computational speeds that meet requirements in most tasks, their black-box characteristics and limited generalization capability seriously affect their reliability and precision in solving scientific problems, and thus cannot yet serve as a mature solution to completely replace traditional numerical algorithms.

In fact, from a computational perspective, there is no essential difference between machine learning and numerical simulation. Therefore, we note that the machine learning frameworks' powerful optimization capabilities and low development threshold are expected to significantly improve the efficiency of numerical compu-

tation. As an application, this paper proposes **PyTorch-TensorRT-EFIT** (PTEFIT), a GPU-parallel numerical algorithm in plasmas equilibrium reconstruction algorithm based on physical principles, constructed and inferred using machine learning frameworks PyTorch[1] and TensorRT[2]. PTEFIT takes advantages of PyTorch's modular characteristic in algorithm construction, which enables the algorithm to flexibly handle different configurations encountered in real-time; the constructed PyTorch modules can be automatically converted to TensorRT engine through Open Neural Network Exchange (ONNX)[3]. The automatic optimization during TensorRT engine building can completely replace manual optimization of GPU parallel computing programs. Ultimately, PTEFIT achieves a computation time of only approximately 0.268 ms for a single time slice at 129×129 resolution, $\sim 10^4 \times$ faster than offline EFIT and about $2 \sim 10 \times$ faster than traditional GPU-accelerated reconstruction.

For tokamak-based controlled fusion, equilibrium reconstruction refers to the algorithm that solves for the internal state and distribution of plasmas using measurement data provided in real-time by diagnostics under the axisymmetric approximation. The basic principle of equilibrium reconstruction is to solve the Grad-Shafranov (G-S) equation[4, 5]

$$\Delta^* \Psi = -\mu_0 R J_\phi = -\mu_0 R^2 \frac{dP}{d\Psi} - \mu_0^2 F \frac{dF}{d\Psi} \quad (1)$$

to obtain the poloidal magnetic flux distribution Ψ from the toroidal current density J_ϕ . In the equation, the Laplacian operator $\Delta^* = R^2 \nabla \cdot (\nabla / R^2)$, R denotes the ra-

dial distance from the symmetry axis, P and F represent the plasmas pressure and poloidal current, respectively. In experiments, J_ϕ is typically pre-divided into several current filaments or parameterized by preset distributions, such that a finite number of quantities can determine its distribution, thereby enabling the solution through constructing a least squares system of equations

$$G_P J_\phi = b - G_C I_C, \quad (2)$$

where G_P is the mutual inductance matrix between the reconstruction region and diagnostic devices; b represents the physical quantities provided by external diagnostics, such as loop flux and poloidal magnetic field; I_C and G_C denote the poloidal field coil currents and their mutual inductance matrices with the diagnostics, respectively. Other quantities such as magnetic field, safety factor, inductance, and beta can be then calculated given Ψ and J_ϕ .

Equilibrium reconstruction is crucial for tokamak experiments, as it can not only be used to analyze discharge quality and guide optimization strategies for subsequent experiments, but also provide real-time plasmas state during discharge for various feedback controls. EFIT (Equilibrium FITting code) is currently the most popular tokamak equilibrium reconstruction algorithm[6], and has been widely used in devices such as DIII-D, EAST, START, HL-2A, HL-3, NSTX, KSTAR, C-MOD, JET, MAST, QUEST, and EXL-50U[7–24]. EFIT solves the G-S equation by repeatedly performing Picard iterations for each time slice, calculating relevant plasmas parameters after convergence is achieved. Although EFIT can adequately handle offline reconstruction tasks, its computation time for a single time slice is on the order of seconds, making it unsuitable for direct use in real-time feedback control during discharge.

Therefore, equilibrium reconstruction is a typical example for those traditional numerical algorithms facing the trouble to balance the computation accuracy and efficiency. There have been several works attempting to optimize the algorithm for improved computational speed, including methods such as reducing grid resolution[25], presetting certain parameters in a specified tokamak that would otherwise be computed in real-time, and implementing parallel computation on GPUs[26–28]. However, each of the aforementioned methods has its own limitations: reducing resolution degrades accuracy to some extent; freezing certain parameters lowers the algorithm's generality across different devices and configurations; traditional GPU programming requires complex manual tuning to achieve optimal performance, and the optimal configuration also varies with grid resolution, hardware devices, and other factors.

In addition to the above works, many studies have also attempted to surrogate equilibrium reconstruction algorithms with deep neural networks[29–43], but still cannot be applied widely in experiments for its inherent limitations mentioned above.

In this case, PTEFIT is developed to satisfy the requirements of real-time tokamak plasmas control in accuracy and efficiency, while also having the capability to handle different flux surface configurations and the potential for cross-device migration. Currently, PTEFIT has been deployed on the EXL-50U spherical tokamak, successfully driving feedback control of the maximum radial position of plasmas and isoflux control, completely meeting the desired performance in experiments, and is general enough to be applied to other algorithms.

In addition to machine learning frameworks-based development, PTEFIT also possesses the following two major features:

- PTEFIT is entirely constructed based on physical principles, thus free from the constraints of black-box and generalization performance of machine learning methods. Compared to other numerical real-time reconstruction works mentioned above, PTEFIT can not only achieve the speed required for real-time operation without reducing resolution, but flexibly adapt to different flux surface configurations as well, and has a lower development and usage threshold.

- PTEFIT adopts algorithmic implementations completely consistent with EFIT wherever possible without affecting real-time performance, and its reconstruction results have been benchmarked against those of EFIT.

The remainder of this paper is organized as follows: Section II introduces the relevant implementation details of PTEFIT; section III evaluates the computational efficiency of PTEFIT and its consistency with EFIT under advanced divertor configurations. Additionally, this section demonstrates the effects of feedback control over the maximum horizontal position of plasmas and isoflux control with PTEFIT participation; finally, section IV summarizes our work and provides an outlook for future development.

PTEFIT follows the tokamak coordinate system convention $COCOS = 7$ [44], and all performance evaluations in this paper were conducted on an NVIDIA(R) RTX 4090 GPU device.

II. METHODS

PTEFIT is modularly constructed utilizing PyTorch features, comprising 21 computational modules, each of which can operate independently. The primary roles for these modules in reconstruction include generating Green's function matrices, determining current density parameters, solving G-S equations, calculating flux surface averaged quantities, etc. The section mainly introduces the implementation principles and optimization methods of them.

A. Green's Function Matrices Generation

In equilibrium reconstruction, the Green's function matrices relate the toroidal current to the poloidal field (magnetic field or flux) it produces. In a coordinate system composed of R, Z in the poloidal plane, the contributions to the poloidal magnetic field B and flux ψ at (r', z') from a toroidal current filament intersecting the poloidal plane at (r, z) are respectively

$$B_r = \frac{\mu_0 I}{4\pi} \int_0^{2\pi} \frac{r'(z-z') \cos \varphi d\varphi}{\sqrt{(z-z')^2 + (r-r' \cos \varphi)^2 + (r' \sin \varphi)^2}^3}, \quad (3)$$

$$B_z = \frac{\mu_0 I}{4\pi} \int_0^{2\pi} \frac{(r'^2 - rr' \cos \varphi) d\varphi}{\sqrt{(z-z')^2 + (r-r' \cos \varphi)^2 + (r' \sin \varphi)^2}^3}, \quad (4)$$

and

$$\psi = \frac{\mu_0 I}{4\pi} \int_0^{2\pi} \frac{rr' \cos \varphi d\varphi}{\sqrt{(z-z')^2 + (r-r' \cos \varphi)^2 + (r' \sin \varphi)^2}}, \quad (5)$$

where I is the current carried by the filament and φ represents the toroidal angle. The entire calculation involves only element-wise and reduce sum operations as long as computing the elliptic integrals by cumulative summation, which can be transformed into highly parallel matrix multiplications. Optimized by PyTorch's native GPU acceleration based on the CUDA backend, PTEFIT generates all Green's function matrices in only approximately 15s at 129×129 resolution, while EFIT requires about 15 minutes. The Green's function matrices can be pre-generated and have no real-time requirements as they are only related to presetting parameters such as tokamak geometry and reconstruction region.

B. Response Matrix and Least Squares Solution

The plasmas toroidal current density J_φ can always be written as the direct product of a matrix \mathbf{J}_b and undetermined coefficients X whether by the current filament division or the parameterization. Substituting into equation 2 yields

$$\mathfrak{R}X = b - G_C I_C, \quad (6)$$

which can also be expressed as

$$\begin{bmatrix} \mathfrak{R} \\ G_C \end{bmatrix} \begin{bmatrix} X \\ I'_C \end{bmatrix} = \begin{bmatrix} b \\ I_C \end{bmatrix} \quad (7)$$

while considering the coil currents as free parameters, from which $\mathfrak{R} = G_P \mathbf{J}_b$ is the response matrix and I'_C is

the inverted coil current, respectively. Compared to the measured coil currents I_C , I'_C is obtained through joint optimization with other diagnostics, which can not only equivalently account for the effects of vacuum vessel induced currents to some extent, but also mitigate the vertical displacement of plasmas caused by Picard iteration. The construction of \mathfrak{R} involves only trivial matrix multiplications and can therefore be efficiently completed by GPU.

In PTEFIT, J_φ is parameterized in polynomial by assuming the forms of P' and FF' within the plasmas boundary are

$$P' = \sum_{i=0}^{N_{P'}} a_i (\tilde{\Psi}^i - \tilde{\Psi}^{N_{P'}}) \quad (8)$$

and

$$FF' = \sum_{j=0}^{N_{FF'}} b_j (\tilde{\Psi}^j - \tilde{\Psi}^{N_{FF'}}), \quad (9)$$

which is consistent with EFIT. From equation 1, \mathbf{J}_b and X can be expressed as

$$\mathbf{J}_b = \left(R(1 - \tilde{\Psi}^{N_{P'}}), R(\tilde{\Psi} - \tilde{\Psi}^{N_{P'}}), \dots, \frac{\mu_0}{R}(1 - \tilde{\Psi}^{N_{FF'}}), \dots, \frac{\mu_0}{R}(\tilde{\Psi}^{N_{FF'}-1} - \tilde{\Psi}^{N_{FF'}}) \right) \quad (10)$$

and

$$X = (a_0, a_1, \dots, a_{N_{P'}}, b_0, b_1, \dots, b_{N_{FF'}})^T, \quad (11)$$

respectively, where $\tilde{\Psi}$ is the normalized flux, $N_{P'}$ and $N_{FF'}$ are the maximum polynomial orders of P' and FF' , respectively. Therefore, solving for J_φ requires first calculating the fluxes at the axis and boundary, as well as a boolean matrix representing the plasmas existence region, which will be discussed in section II D.

PTEFIT provides two methods for solving the least squares equations: constructing normal equations and QR decomposition by Gram-Schmidt orthogonalization. One should be pointed that PTEFIT does not employ the singular value decomposition (SVD) method used in EFIT, because the rounding errors induced by SVD is unacceptable in single-precision floating point number, which is generally operated in GPU. It can be shown that the QR decomposition based on Gram-Schmidt orthogonalization is numerically stable[45], but requires longer computation time; constructing and solving normal equations is faster but causes the increasing condition number of the coefficient matrices, making it suitable for cases where the dimension of X is relatively low.

C. Solution of G-S Equation

The G-S equation can be transformed through finite differences into a $(N_R - 2) \times (N_Z - 2)$ dimensional pentadiagonal matrix equation with Dirichlet boundary conditions, where N_R and N_Z represent the number of grid points in the R and Z directions, respectively. Directly solving the equation incurs enormous computational overhead, but it can be transformed into $N_Z - 2$ tridiagonal matrix equations to solve in parallel, where the coefficient matrices can be pre-computed. Detailed principles can be found in reference[27].

D. Processing on Flux Surface

The flux surfaces solved from the G-S equation must be processed to obtain the normalized flux Ψ and the plasmas existence region for constructing \mathbf{J}_b , as mentioned in section II B above.

The normalized flux distribution can be derived by computing flux values at the magnetic axis and boundary of the plasmas. For divertor configurations, the axis and boundary correspond to an O-point and an X-point in the flux distribution, both of them are extremal points satisfying $\nabla\Psi = 0$. Furthermore, the Hessian matrix \mathbf{H} at O-points and X-points satisfies $\det\mathbf{H} > 0$ and $\det\mathbf{H} < 0$, respectively. Notably, it is impossible to find grid points where $\nabla\Psi$ is exactly 0 in a discretized flux distribution, and alternative schemes based on sign comparison of finite difference products may fail due to non-uniform flux variation in different directions near X-points. To address this, a second-order polynomial fitting, which formally allows for the existence of O-points and X-points, is utilized in the vicinity of each grid point, enabling exact analytical solutions where $\nabla\Psi = 0$. Meanwhile, under the parameterized distribution, the Hessian matrix \mathbf{H} has a simple form and is easy to compute.

Polynomial fitting requires solving $(N_R - 2) \times (N_Z - 2)$ least squares equations, but since the grid point distribution is fixed, the algorithm only needs to perform matrix multiplications for this step in real-time by pre-constructing normal equations and inverting the coefficient matrices.

The flux varies monotonically from the magnetic axis to the boundary within the plasmas region, but exhibits complex behavior outside the last closed flux surface (LCFS). Therefore, the plasmas existence region must be identified first to find the axis and boundary from all O- and X-points. PTEFIT employs the same principle as described in reference[25] to determine the plasmas region, but executes in parallel on the GPU.

For limiter configurations, the plasmas boundary is not located at an X-point. However, for any single plasma blob, the boundary flux can be determined by comparing the flux values of all limiter vertices and X-points within the plasmas region.

For doublet and droplet configurations, only the flux at

limiter positions is compared when selecting the boundary, which can be achieved by appending a value with very large absolute magnitude and sign opposite to I_P to X-point fluxes during comparison.

E. Flux Surface Averaged Quantities

Flux surface averaged quantities, including the safety factor, are crucial for plasmas transport and confinement performance, and therefore need to be computed rapidly for subsequent real-time control requirements. A flux surface averaged quantity Q can be expressed as a specific integral form along a closed flux surface:

$$Q_{\mu,\nu} = \oint_l |\nabla\Psi|^\mu R^\nu dl, \quad (12)$$

where l is the poloidal path along a certain closed flux surface, and μ, ν are arbitrary integers. In particular, the safety factor can be expressed as $q = \frac{\mu_0 F}{2\pi} Q_{-1,-2}$. The only difficulty in computing $Q_{\mu,\nu}$ lies in obtaining the poloidal path l of the closed flux surface.

PTEFIT adopts the bisection method to determine flux surface vertices. By filtering the flux outside the plasmas region using the boolean matrix obtained in section II D, the flux monotonicity required by the bisection method is guaranteed. As shown in figure 1, the bisection method can efficiently take advantages of GPU parallel characteristic, with each thread processing one chord. The initial endpoints are taken at the magnetic axis and a point on the reconstructed boundary, respectively. After each search, linear interpolation is performed to obtain the new vertex flux. It should be noted that the initial vertices taken on the reconstructed boundary must be arranged continuously in clockwise/counterclockwise order to ensure the flux surface element dl can be correctly computed subsequently. Under typical device scales, only about 10 iterations are needed to reduce the flux surface error to approximately 1mm, which is sufficient considering the error impact from linear interpolation. After obtaining the flux surface vertices, the subsequent geometric parameters of the plasmas (minor radius, elongation, etc.) and global parameters (beta, internal inductance, stored energy) can also be derived through simple calculations.

PTEFIT can also search for flux surfaces under doublet or droplet configurations through appropriate selection of iteration initial endpoints and additional filtering operations. Details are not elaborated in this article.

F. Optimization

In addition to parallelization, the main optimization techniques employed by PTEFIT during algorithm construction are as follows:

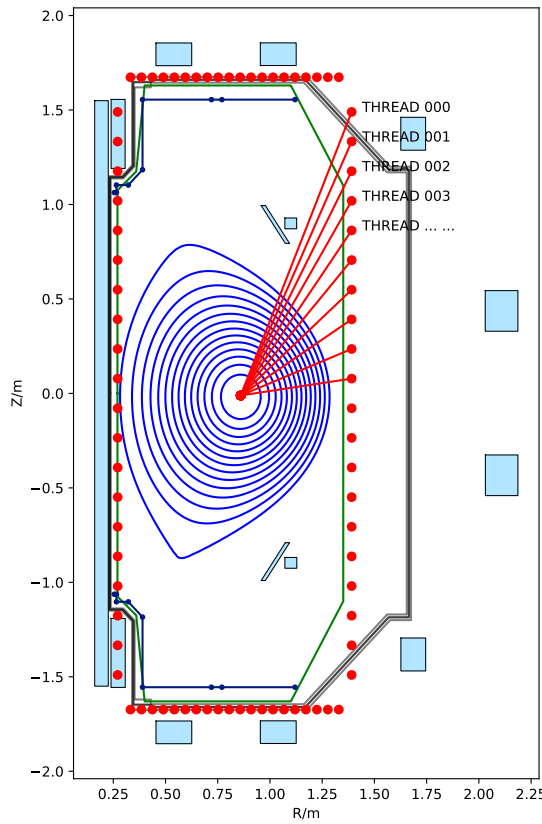


FIG. 1: Schematic diagram of the bisection method for finding flux surface vertices. The flux outside the plasma region need to be filtered first. For each thread, the initial endpoints are located at the magnetic axis and the reconstructed boundary, respectively, and the points on the reconstructed boundary must be arranged continuously in clockwise or counterclockwise order.

1. PTEFIT is based on the slow flux variation assumption, performing only one Picard iteration per time slice during a continuous discharge.
2. To ensure that the algorithm can be fully captured as a CUDA graph, boolean variables and multiply-add operations are used instead of conditional statements to avoid potential graph non-determinism. Operators that cannot be captured as CUDA graphs have been rebuilt to TensorRT custom plugins to explicitly define their behavior.
3. All data that can be pre-computed before discharge are computed in advance and frozen in real-time to improve efficiency.
4. The entire computation flow is defined to execute on the GPU to reduce data transfer latency, from which division and square root operations are avoided wherever possible. Memory, cache, and thread optimizations are automatically completed by TensorRT.

III. RESULTS

A. Consistency with Offline EFIT

We selected the XPT (X-Point Target) configuration recently successfully achieved on the EXL-50U spherical tokamak[46, 47] to compare the consistency between PTEFIT and offline EFIT. Figures 2(a)(c) compare the LCFS obtained by PTEFIT and offline EFIT for two time slices in shot #13899, from which PTEFIT and EFIT show high consistency in both X-divertor minus and X-divertor plus configurations, with the LCFS reconstruction deviation controlled to approximately 1cm. Notably, due to the computational speed limitations, inter-shot offline EFIT can only operate reconstruction at a time slice period of 10ms, potentially missing certain important experimental phenomena; while PTEFIT computes in real-time at 1kHz resolution during discharge, enabling observation of critical moments such as the transition from X-divertor minus to X-divertor plus immediately after discharge (figure 2(b)).

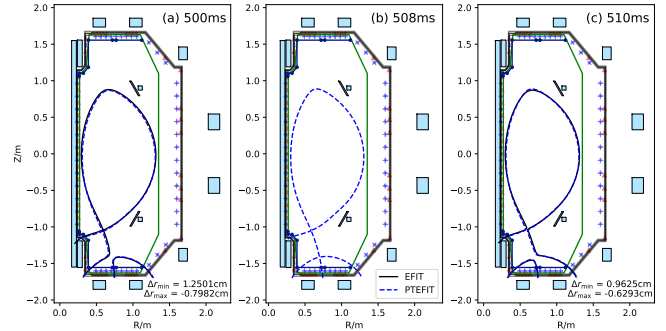


FIG. 2: Comparison of LCFS results obtained by PTEFIT and offline EFIT for XPT configuration reconstruction of shot #13899. Here, Δr_{\min} and Δr_{\max} are the deviations between the two at the minimum and maximum radial positions of the LCFS, respectively.

B. Computation Efficiency

PTEFIT has achieved sub-millisecond computational speed with 0.268ms average computation time per slice under the configuration of 129×129 grid resolution, 33 profile points, and normal equation construction as the least squares driver. Figure 3 shows the distribution of PTEFIT computation speed over 10,000 consecutive time slices.

C. Feedback Control over R_{\max}

Maintaining the maximum radial position R_{\max} of plasma stable is crucial for ion cyclotron range of frequencies (ICRF) heating[48]. During ICRF experiments on

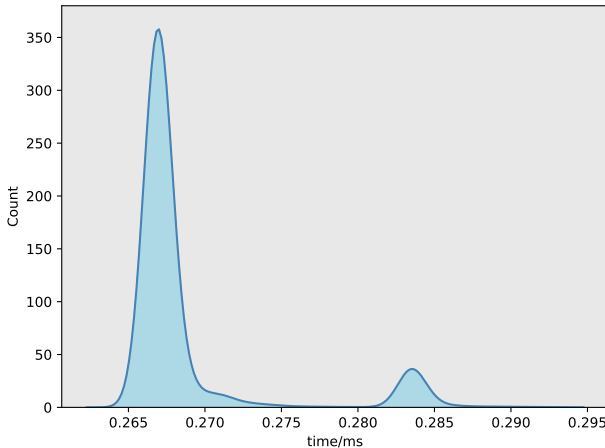


FIG. 3: Distribution of PTEFIT computation time per time slice.

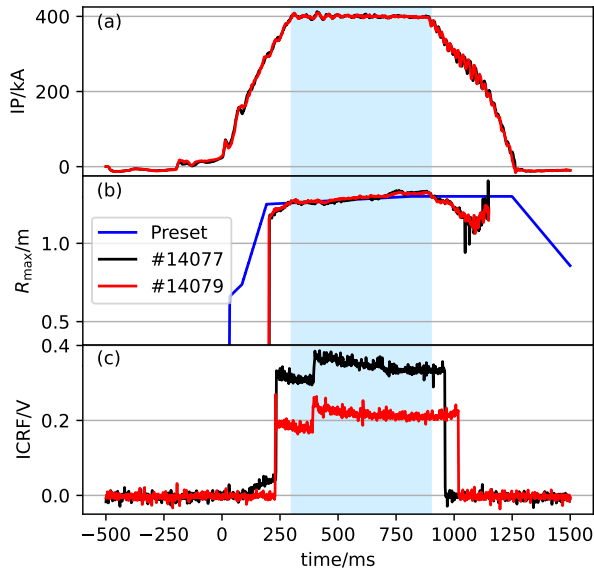


FIG. 4: Demonstration of PID feedback control effects using the maximum radial position R_{\max} of plasmas provided in real-time by PTEFIT for two shots. (a) Plasmas current waveform. (b) Preset R_{\max} and R_{\max} obtained from PTEFIT real-time reconstruction. (c) ICRF intensity waveform.

EXL-50U, PTEFIT provides R_{\max} in real-time, enabling proportional-integral-derivative (PID) feedback control. Figure 4 shows two shots of discharge with R_{\max} control driven by PTEFIT, where different intensities of ICRF heating were applied. As shown in figure 4(b), during the current flat-top period, the PTEFIT-driven R_{\max} feedback control can maintain the target deviation at approximately 2cm.

D. Isoflux Control

Isoflux control refers to the multi-input multi-output (MIMO) feedback control by observing the flux difference between LCFS and preset reference points. Figure 5 shows the waveforms and isoflux control effects of EXL-50U shot #14488.

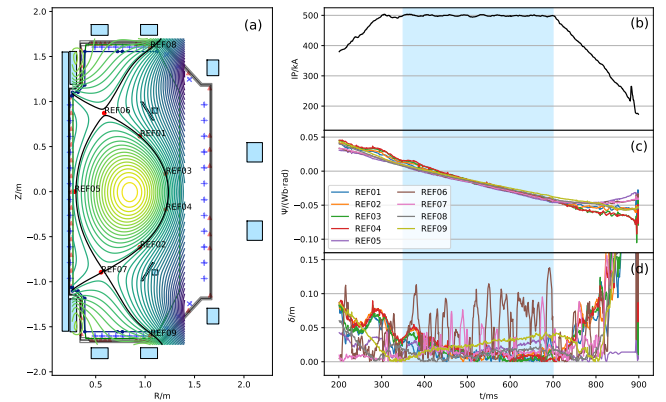


FIG. 5: Schematic diagram of isoflux control for shot #14488. (a) Flux surface distribution at 600 ms. (b) Plasmas current waveform. (c) Temporal evolution of flux at each reference point. (d) Temporal evolution of distance between each reference point and the LCFS. The background is light blue during the isoflux control period.

In this shot, isoflux control takes over from 350ms to 700ms. Among them, the red dots are the preset reference points, including 2 reference divertor strike points, 2 reference X-points, and 5 other reference points located on the LCFS. Figures 5(b)(c)(d) sequentially show the plasma current, the flux at each reference point, and the distance from the LCFS. During isoflux control, it can be seen that the flux values at each reference point are nearly identical, and the distance between each reference point (except X-points) and the LCFS averages approximately 2cm. However, due to the influence of vertical displacement events (VDEs), only one of the two X-points can be located on the LCFS at the same time. VDEs grow so rapidly that isoflux control at a period of 1ms is not sufficient to suppress this instability. The improved future work combining vertical displacement control with isoflux control may be considered to mitigate the problem.

IV. SUMMARY

Based on physical principles, we take advantages of machine learning frameworks to optimize numerical algorithms, implementing the real-time reconstruction algorithm PTEFIT, which is constructed in PyTorch and executes in real-time under TensorRT. PTEFIT has been successfully deployed on the EXL-50U spherical tokamak to support experiments including XPT configura-

tion discharges, ICRF, and isoflux control. Leveraging the Python API and inherent modularity provided by PyTorch, the algorithm has an extremely low development and usage threshold, and is easy for migration; the automatic optimization and C++ API of TensorRT further reduce development difficulty while ensuring real-time performance and compatibility, ultimately achieving an average reconstruction time of 0.268 ms for single time slice.

PTEFIT maintains consistency with EFIT in both algorithm and principle wherever possible, and is benchmarked against EFIT results, with the reconstructed LCFS showing an average deviation of approximately 1cm from offline EFIT. In terms of real-time deployment, both the control targeting plasmas radial position and the isoflux maintain the accuracy of approximately 2cm.

Although PTEFIT's computational efficiency already meets experimental requirements, the results need to be transferred to CPU and then sent to the control system via reflective memory for feedback control, leaving room for improvement in the overall latency. Future work may consider integrating the feedback control al-

gorithm into PTEFIT to directly output coil voltages for improved computational efficiency. Additionally, it is also meaningful to combine kinetic diagnostics with integrated modeling to calculate accurate profiles, which could be applied to profile feedback control and other experiments.

Finally, we believe that PTEFIT and its design philosophy, which taking fully advantages of mutual machine learning frameworks for numerical optimization, have sufficient generalization capabilities applicable to most traditional numerical algorithms efficiently.

ACKNOWLEDGMENTS

This work is supported by National Natural Science Foundation of China under Grant No.12275142 and No.12275354, National MCF Energy R&D Program under Grant No.2024YFE03020001. Besides, we are particularly grateful to ENN for the scientific research funding supporting this study.

[1] Jason Ansel, Edward Yang, Horace He, Natalia Gimelshein, Animesh Jain, Michael Voznesensky, Bin Bao, Peter Bell, David Berard, Evgeni Burovski, Geeta Chauhan, Anjali Chourdia, Will Constable, Alban Desmaison, Zachary DeVito, Elias Ellison, Will Feng, Jiong Gong, Michael Gschwind, Brian Hirsh, Sherlock Huang, Kshiteej Kalambarkar, Laurent Kirsch, Michael Lazos, Mario Lezcano, Yanbo Liang, Jason Liang, Yinghai Lu, C. K. Luk, Bert Maher, Yunjie Pan, Christian Puhrsch, Matthias Reso, Mark Saroufim, Marcos Yukio Siraichi, Helen Suk, Shunting Zhang, Michael Suo, Phil Tillet, Xu Zhao, Eikan Wang, Keren Zhou, Richard Zou, Xiaodong Wang, Ajit Mathews, William Wen, Gregory Chanan, Peng Wu, and Soumith Chintala. PyTorch 2: Faster Machine Learning Through Dynamic Python Bytecode Transformation and Graph Compilation. In *Proceedings of the 29th ACM International Conference on Architectural Support for Programming Languages and Operating Systems, Volume 2*, volume 2 of *ASPLOS '24*, pages 929–947, New York, NY, USA, April 2024. Association for Computing Machinery.

[2] Github - NVIDIA/TensorRT. (available at <https://github.com/NVIDIA/TensorRT>).

[3] Github - onnx/onnx. (available at <https://github.com/onnx/onnx>).

[4] Harold Grad and Hanan Rubin. Hydromagnetic equilibria and force-free fields. *Journal of Nuclear Energy* (1954), 7(3-4):284–285, September 1958.

[5] Huasheng Xie and Yueyan Li. What Is the Minimum Number of Parameters Required to Represent Solutions of the Grad-Shafranov Equation?, January 2026. arXiv:2601.02942 [physics].

[6] L.L. Lao, H. St. John, R.D. Stambaugh, A.G. Kellman, and W. Pfeiffer. Reconstruction of current profile parameters and plasma shapes in tokamaks. *Nuclear Fusion*, 25(11):1611, November 1985.

[7] J W Berkery, S A Sabbagh, L Kogan, D Ryan, J M Bialek, Y Jiang, D J Battaglia, S Gibson, and C Ham. Kinetic equilibrium reconstructions of plasmas in the MAST database and preparation for reconstruction of the first plasmas in MAST upgrade. *Plasma Physics and Controlled Fusion*, 63(5):055014, April 2021. Publisher: IOP Publishing.

[8] H. Lian, H.Q. Liu, K. Li, Z.Y. Zou, J.P. Qian, M.Q. Wu, G.Q. Li, L. Zeng, Q. Zang, B. Lv, Y.X. Jie, and EAST team. EAST kinetic equilibrium reconstruction combining with Polarimeter-Interferometer internal measurement constraints. *Journal of Instrumentation*, 12(12):C12036, December 2017.

[9] G Q Li, Q L Ren, J P Qian, L L Lao, S Y Ding, Y J Chen, Z X Liu, B Lu, and Q Zang. Kinetic equilibrium reconstruction on EAST tokamak. *Plasma Physics and Controlled Fusion*, 55(12):125008, November 2013. Publisher: IOP Publishing.

[10] Xuexi Zhang, Guoqiang Li, and Torrin Bechtel Amara. Reconstruction of current profiles from external magnetic and MSE measurements on DIII-D. *Nuclear Fusion*, 66(1):016015, November 2025. Publisher: IOP Publishing.

[11] L.L. Lao, J.R. Ferron, R.J. Groebner, W. Howl, H. St. John, E.J. Strait, and T.S. Taylor. Equilibrium analysis of current profiles in tokamaks. *Nuclear Fusion*, 30(6):1035, June 1990.

[12] D. P. O'Brien, L. L. Lao, E. R. Solano, M. Garibba, T. S. Taylor, J. G. Cordey, and J. J. Ellis. Equilibrium analysis of iron core tokamaks using a full domain method. *Nuclear Fusion*, 32(8):1351, August 1992.

[13] Lao, LL, John, HE St, Peng, Q, Ferron, JR, Strait, EJ, Taylor, TS, Meyer, WH, Zhang, C, and You, KI. MHD equilibrium reconstruction in the DIII-D tokamak.

Fusion science and technology, 48(2):968–977, 2005.

[14] S. A. Sabbagh, S. M. Kaye, J. Menard, F. Paoletti, M. Bell, R. E. Bell, J. M. Bialek, M. Bitter, E. D. Fredrickson, D. A. Gates, A. H. Glasser, H. Kugel, L. L. Lao, B. P. LeBlanc, R. Maingi, R. J. Maqueda, E. Mazzucato, D. Mueller, M. Ono, S. F. Paul, M. Peng, C. H. Skinner, D. Stutman, G. A. Wurden, W. Zhu, and NSTX Research Team. Equilibrium properties of spherical torus plasmas in NSTX. *Nuclear Fusion*, 41(11):1601, November 2001.

[15] Qian Jinping, Wan Baonian, L. L. Lao, Shen Biao, S. A. Sabbagh, Sun Youwen, Liu Dongmei, Xiao Bingjia, Ren Qilong, Gong Xianzu, and Li Jiangang. Equilibrium Reconstruction in EAST Tokamak. *Plasma Science and Technology*, 11(2):142, April 2009.

[16] Y.S. Park, S.A. Sabbagh, J.W. Berkery, J.M. Bialek, Y.M. Jeon, S.H. Hahn, N. Eidietsis, T.E. Evans, S.W. Yoon, J.-W. Ahn, J. Kim, H.L. Yang, K.-I. You, Y.S. Bae, J. Chung, M. Kwon, Y.K. Oh, W.-C. Kim, J.Y. Kim, S.G. Lee, H.K. Park, H. Reimerdes, J. Leuer, and M. Walker. KSTAR equilibrium operating space and projected stabilization at high normalized beta. *Nuclear Fusion*, 51(5):053001, April 2011.

[17] Y. Jiang, S.A. Sabbagh, Y.S. Park, J.W. Berkery, J.H. Ahn, J.D. Riquezes, J.G. Bak, W.H. Ko, J. Ko, J.H. Lee, S.W. Yoon, A.H. Glasser, and Z.R. Wang. Kinetic equilibrium reconstruction and the impact on stability analysis of KSTAR plasmas. *Nuclear Fusion*, 61(11):116033, October 2021. Publisher: IOP Publishing.

[18] L. C. Appel, M. K. Bevir, and M. J. Walsh. Equilibrium reconstruction in the START tokamak. *Nuclear Fusion*, 41(2):169, February 2001.

[19] Y. In, J. J. Ramos, A. E. Hubbard, I. H. Hutchinson, M. Porkolab, J. Snipes, S. M. Wolfe, and A. Bondeson. Resistive $n = 1$ modes in reversed magnetic shear Alcator C-Mod plasmas. *Nuclear Fusion*, 40(8):1463, August 2000.

[20] W. Zwingmann. Equilibrium analysis of steady state tokamak discharges. *Nuclear Fusion*, 43(9):842, August 2003.

[21] Li, YG, Lotte, Ph, Zwingmann, W, Gil, C, and Imbeaux, F. EFIT equilibrium reconstruction including polarimetry measurements on tore supra. *Fusion science and technology*, 59(2):397–405, 2011.

[22] He Hongda, Zhang Jinhua, Dong Jiaqi, and Li Qiang. Study of Plasma MHD Equilibrium in HL-2A Tokamak. *Plasma Science and Technology*, 8(4):397, July 2006.

[23] Erbing Xue, Xianmei Zhang, Kazuo Nakamura, and Limin Yu. Equilibrium Reconstruction and Equilibrium Properties in QUEST Tokamak. *Journal of Fusion Energy*, 38(2):244–252, April 2019.

[24] Appel, LC, Huysmans, GTA, Lao, LL, McCarthy, PJ, Muir, DG, Solano, ER, Storrs, J, Taylar, D, Zwingmann, W, and others. A unified approach to equilibrium reconstruction. In 33rd EPS Conference on Plasma Physics 2006, pages p-2.160, Rome, Italy, June 2006.

[25] J. M. Moret, B. P. Duval, H. B. Le, S. Coda, F. Felici, and H. Reimerdes. Tokamak equilibrium reconstruction code LIUQE and its real time implementation. *Fusion Engineering and Design*, 91:1–15, February 2015.

[26] Yao Huang, Bing-Jia Xiao, and Zheng-Ping Luo. Fast parallel Grad-Shafranov solver for real-time equilibrium reconstruction in EAST tokamak using graphic processing unit*. *Chinese Physics B*, 26(8):085204, August 2017.

Publisher: Chinese Physical Society and IOP Publishing Ltd.

[27] Y. Huang, Z.P. Luo, B.J. Xiao, L.L. Lao, A. Mele, A. Pironti, M. Mattei, G. Ambrosino, Q.P. Yuan, Y.H. Wang, and N.N. Bao. GPU-optimized fast plasma equilibrium reconstruction in fine grids for real-time control and data analysis. *Nuclear Fusion*, 60(7):076023, June 2020. Publisher: IOP Publishing.

[28] Rui MA, Fan XIA, Fei LING, and Jiaxian LI. Acceleration optimization of real-time equilibrium reconstruction for HL-2A tokamak discharge control. *Plasma Science and Technology*, 20(2):025601, January 2018. Publisher: IOP Publishing.

[29] Matteo Bonotto, Domenico Abate, and Leonardo Piggatto. Reconstruction of plasma equilibrium and separatrix using convolutional physics-informed neural operator. *Fusion Engineering and Design*, 200:114193, March 2024.

[30] J. McClenaghan, C. Akçay, T. B. Amara, X. Sun, S. Madireddy, L. L. Lao, S. E. Kruger, and O. M. Meneghini. Augmenting machine learning of Grad-Shafranov equilibrium reconstruction with Green's functions. *Physics of Plasmas*, 31(8):082507, August 2024.

[31] Jingjing Lu, Youjun Hu, Nong Xiang, and Youwen Sun. Fast equilibrium reconstruction by deep learning on EAST tokamak. *AIP Advances*, 13(7):075007, July 2023.

[32] Semin Joung, Jaewook Kim, Sehyun Kwak, J.G. Bak, S.G. Lee, H.S. Han, H.S. Kim, Geunho Lee, Daeho Kwon, and Y.-C. Ghim. Deep neural network Grad-Shafranov solver constrained with measured magnetic signals. *Nuclear Fusion*, 60(1):016034, December 2019. Publisher: IOP Publishing.

[33] L L Lao, S Kruger, C Akçay, P Balaprakash, T A Bechtel, E Howell, J Koo, J Leddy, M Leinhauser, Y Q Liu, S Madireddy, J McClenaghan, D Orozco, A Pankin, D Schissel, S Smith, X Sun, and S Williams. Application of machine learning and artificial intelligence to extend EFIT equilibrium reconstruction. *Plasma Physics and Controlled Fusion*, 64(7):074001, June 2022. Publisher: IOP Publishing.

[34] S. Madireddy, C. Akçay, S. E. Kruger, T. Bechtel Amara, X. Sun, J. McClenaghan, J. Koo, A. Samaddar, Y. Liu, P. Balaprakash, and L. L. Lao. EFIT-Prime: Probabilistic and physics-constrained reduced-order neural network model for equilibrium reconstruction in DIII-D. *Physics of Plasmas*, 31(9):092505, September 2024.

[35] Yuri V. Mitrishkin, Pavel S. Korenev, Artem E. Konkov, Valerii I. Kruzhkov, Nicolai E. Ovsiannikov, Yuri V. Mitrishkin, Pavel S. Korenev, Artem E. Konkov, Valerii I. Kruzhkov, and Nicolai E. Ovsiannikov. New Identification Approach and Methods for Plasma Equilibrium Reconstruction in D-Shaped Tokamaks. *Mathematics*, 10(1), December 2021. Company: Multidisciplinary Digital Publishing Institute Distributor: Multidisciplinary Digital Publishing Institute Institution: Multidisciplinary Digital Publishing Institute Label: Multidisciplinary Digital Publishing Institute Publisher: publisher.

[36] Semin Joung, Y.-C. Ghim, Jaewook Kim, Sehyun Kwak, Daeho Kwon, C. Sung, D. Kim, Hyun-Seok Kim, J. G. Bak, and S. W. Yoon. GS-DeepNet: mastering tokamak plasma equilibria with deep neural networks and the Grad-Shafranov equation. *Scientific Reports*,

13(1):15799, September 2023. Publisher: Nature Publishing Group.

[37] J.T. Wai, M.D. Boyer, and E. Kolemen. Neural net modeling of equilibria in NSTX-U. *Nuclear Fusion*, 62(8):086042, July 2022. Publisher: IOP Publishing.

[38] Chenguang Wan, Zhi Yu, Alessandro Pau, Olivier Sauter, Xiaojuan Liu, Qiping Yuan, and Jiangang Li. A machine-learning-based tool for last closed-flux surface reconstruction on tokamaks. *Nuclear Fusion*, 63(5):056019, April 2023. Publisher: IOP Publishing.

[39] G.H. Zheng, Z.Y. Yang, S.F. Liu, R. Ma, X.W. Gong, A. Wang, S. Wang, and W.L. Zhong. Real-time equilibrium reconstruction by multi-task learning neural network based on HL-3 tokamak. *Nuclear Fusion*, 64(12):126041, October 2024. Publisher: IOP Publishing.

[40] G.H. Zheng, S.F. Liu, H.S. Xie, X. Gu, Z.Y. Chen, X.C. Lun, Y. Liu, J. Li, D. Guo, R.Y. Tao, H.Y. Zhao, Y.P. Zhang, T.T. Sun, Y.N. Xu, Y.J. Hu, and Z.Y. Yang. EFIT-mini: an embedded, multi-task neural network-driven equilibrium inversion algorithm. *Nuclear Fusion*, 65(10):106008, September 2025. Publisher: IOP Publishing.

[41] Cuizhi Zhou and Kaien Zhu. Physics-Informed Neural Networks for High-Precision Grad-Shafranov Equilibrium Reconstruction, July 2025. arXiv:2507.16636 [physics].

[42] Siqi Ding, Zitong Zhang, Guoyang Shi, Xingyu Li, Xiang Gu, Yanan Xu, Huasheng Xie, Hanyue Zhao, Yuejiang Shi, and Tianyuan Liu. Physics-informed Neural Operator Learning for Nonlinear Grad-Shafranov Equation, November 2025. arXiv:2511.19114 [physics].

[43] Federico Fiorenza, Sara Dubbioso, Gianmaria De Tommasi, and Alfredo Pironti. CARONTE: a Physics-Informed Extreme Learning Machine-Based Algorithm for Plasma Boundary Reconstruction in Magnetically Confined Fusion Devices, December 2025. arXiv:2512.16689 [physics].

[44] O. Sauter and S. Yu. Medvedev. Tokamak coordinate conventions: COCOS. *Computer Physics Communications*, 184(2):293–302, February 2013.

[45] Åke Björck. Solving linear least squares problems by Gram-Schmidt orthogonalization. *BIT Numerical Mathematics*, 7(1):1–21, March 1967.

[46] Yuejiang SHI, Xianming SONG, Dong GUO, Xinchen JIANG, Xiang GU, Lili DONG, Xueyun WANG, Tiantian SUN, Muzhi TAN, Zhengyuan CHEN, Guang YANG, Danke YANG, Huasheng XIE, Hanyue ZHAO, Yong LIU, Renyi TAO, Jia LI, Songjian LI, Fan GAO, Yihang ZHAO, Yupeng ZHANG, Cong ZHANG, Hongda HE, Enwu YANG, Yuanming YANG, Yu WANG, Shaodong SONG, Lei HAN, Bo XING, Pengmin LI, Zhenxing WANG, Peihai ZHOU, Wenwu LUO, Yumin WANG, Bing LIU, Chao WU, Xin ZHAO, Yunfeng LIANG, Jiaqi DONG, Baoshan YUAN, Y-K Martin PENG, Minsheng LIU, and the EXL-50U Team. Strategy and experimental progress of the EXL-50U spherical torus in support of the EHL-2 project. *Plasma Science and Technology*, 27(2):024003, February 2025. Publisher: Plasma Science and Technology.

[47] Yuejiang Shi. Achievement of 1 MA Discharges in Hydrogen-Boron Plasmas on EXL-50U. *Plasma Science and Technology*, 27(9):092002, September 2025. arXiv:2505.08815 [physics].

[48] J.-M. Noterdaeme and G. Van Oost. The interaction between waves in the ion cyclotron range of frequencies and the plasma boundary. *Plasma Physics and Controlled Fusion*, 35(11):1481, November 1993.